MEMS 2001

2001 Microelectromechanical Systems Conference

24–26 August 2001
Berkeley, California, USA

Technical Co-Sponsorship by
IEEE Circuits and Systems Society

IEEE

2001 Microelectromechanical Systems Conference

24–26 August 2001
Berkeley, California, USA

Technical Co-Sponsorship by
IEEE Circuits and Systems Society

2001 Microelectromechanical Systems Conference

Copyright and Reprint Permission

IEEE Catalog Number	01EX521
ISBN	0-7803-7224-7
Library of Congress	2001094657

Additional copies of this publication are available from

IEEE Operations Center
P.O. Box 1331
445 Hoes Lane
Piscataway, NJ 08855-1331 USA

1-800-678-IEEE
1-732-981-1393
1-732-981-9667 (FAX)
email: customer.services@ieee.org

Introduction

MEMS Conference 2001 tooks place August 24 - 26, 2001 at the Berkeley Marina Radisson hotel in Berkeley, California, USA. There were 185 people in attendance representing USA, Canada, Turkey, France, Netherlands, England, Israel, China, Taiwan, Hong Kong and Korea.

The program consisted of 6 technical sessions and a non-technical session. Of 36 submitted papers, 27 were accepted for oral and poster presentations. There were 6 invited speakers. Other elements of the program included a MEMS/MOEMS short course given by Adriatic Research Institute, a simulation workshop given by CFDRC, a panel discussion on venture capital and a vendor session. A technical program committee was responsible for reviewing papers.

Luke P. Lee, General Chair, UC Berkeley, BSAC
Veljko Milanovic, Technical Chair, Adriatic Research Institute

Technical Program Committee

Mona Zaghloul, George Washington University, VP Technical Activities for Circuits and Systems Society
Gabriel Rebeiz, University of Michigan
Olav Solgaard, Stanford University
Michael Cohn, Microassembly Technologies, Inc.
Kumar Subramanian, Phoenix Bioscience
Xiaoning Jiang, Standard MEMS
Angad Singh, Microgen Systems
Zen Chu, Panel discussion coordinator, Net Ventures

The conference received technical co-sponsorship from the IEEE Circuits and Systems Society. The conference was sponsored by Ardesta LLC and Atomasoft Inc. The organizers wish to express their apprectiation for the generous support of these institutions.

The conference was initiated and organized entirely by undergraduate students, led by General Director Ted Strauss. Other organizers were Ben Strauss, Jon Despres, Calin Plesa, David Elkins. Their motivations are best captured by the conference mission statement.

Mission Statement

MEMS Conference has a dual objective. (1) To disseminate current developments of the field by assembling respected individuals from around the world to present current research. (2) To support students, non-profit organizations and start-up companies in the MEMS industry. This is accomplished by making the conference accessible and affordable to these groups, by offering seminars and presentations on topics of particular value to these groups and by donating 20-33% of proceeds towards scholarships and/or non-profit organizations.

(1) was realized as evidenced by this proceedings and by the large number who attended. (2) was realized: there were several students and startups in attendance; 7 student interns assisted with production and were able attended the sessions at no cost; though the conference made no profit, 500$ was donated to UC Berkeley EECS to be used to support students pursuing studies in MEMS.

The organizers would like to thank the many individuals and institutions who contributed to the success of MEMS Conference 2001.

Information about future events is available at www.memsconference.com.

Contents

BioMEMS and Microfluidics Applications of Surface Micromachining Technology

Murat Okandan, Paul Galambos, Sita Mani and Jay Jakubczak.
SANDIA National Laboratories, Albuquerque, N.M.

In the last decade, examples of devices manufactured with SUMMiT technology have demonstrated the capabilities of polysilicon surface micromachining [1]. Currently we are working on enhancements to this technology to enable Microfluidics and BioMEMS. The goal is to ultimately provide functionality that is not feasible with other microfabrication technologies. The enhancements build on the key features of surface micromachining: manufacturability and compatibility with CMOS processing, and allow us to leverage the investment already made in the microelectronics processing technology.

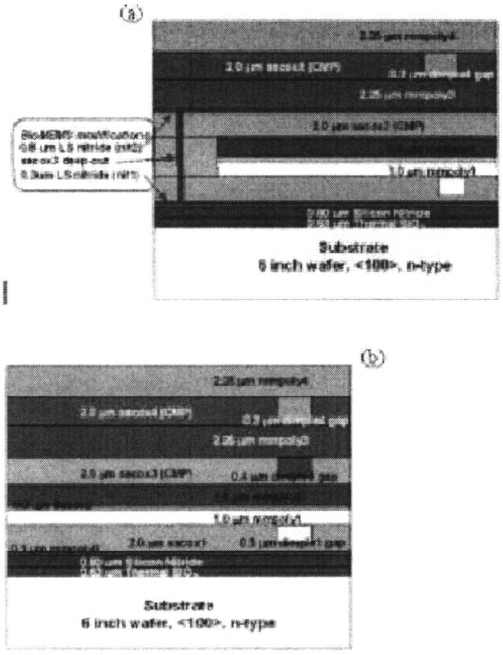

Figure 1: (a) Modified flow and (b) standard SUMMiT layers. The incorporation of the low stress silicon nitride layers allow the creation of complex microfluidic structures and enclosed cavities.

Standard SUMMiT technology uses polysilicon as the mechanical material and silicon dioxide as the sacrificial material (Fig.1b). In this technology, considering each polysilicon layer as a potential microfluidic channel top or bottom, there are 4!=24 possible configurations. We have used standard SUMMiT to fabricate a variety of microfluidic systems; such as a drop ejector (Fig. 2, 2pl drops ejected at 10 m/s [2]) and a peristaltic pump (Fig. 3, 60 nl/s calculated maximum pumping rate for a 0.4 nl volume device [3]). These microfluidic devices highlight an advantage of surface micromachining, the electrostatic actuation system is built directly into the MEMS structure to produce a highly integrated microsystem.

To further enhance the capabilities of our technology, we have developed a new process flow (Fig.1a). In this technology, additional layers of insulating material (low stress silicon nitride) and a deep oxide cut. allow the creation of microfluidic channels, pumps, valves and other enclosures that can be readily interfaced with the extensive library of mechanical components available in the standard technology. These silicon nitride layers also provide optical access into the structures and allow the incorporation of regions of electrical isolation and/or conduction to produce truly integrated electromechanical microfluidic and BioMEMS devices on a chip. By positioning electrodes for creating electric fields and mechanical actuation around the insulated channel the troublesome issue of electrolysis is circumvented.

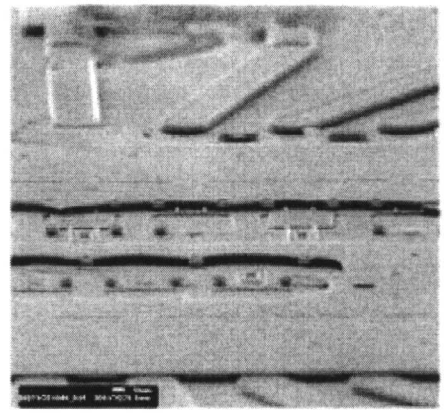

Figure 2: SUMMiT ejector

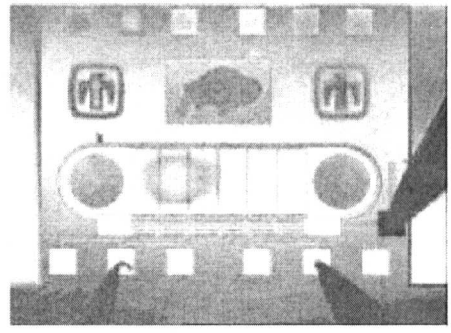

Figure 3: SUMMiT peristaltic pump.

A wafer lot containing designs using the nitride modification was run to test the functionality of both the standard parts and new microfluidic "core-components", such as valves, pumps (Fig.4), mixing/reaction chambers and separation/detection systems. An example of a completed device is shown in Fig. 5, which is a cellular manipulation device. Fig. 6 shows red blood cells flowing through the cellular manipulator.

0-7803-7224-7/02/$17.00 © 2002

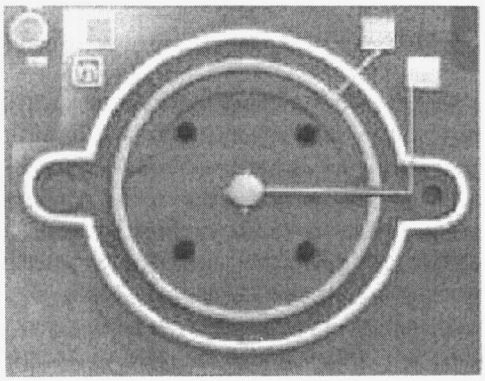

Figure 4: A membrane pump realized using the modified flow. There are inlet/outlet valves inside the cavity and actuation electrodes are placed above the nitride membrane.

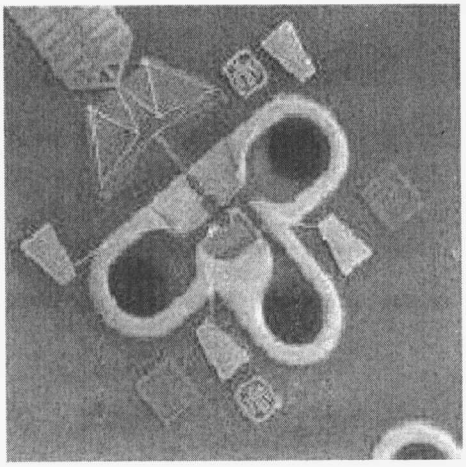

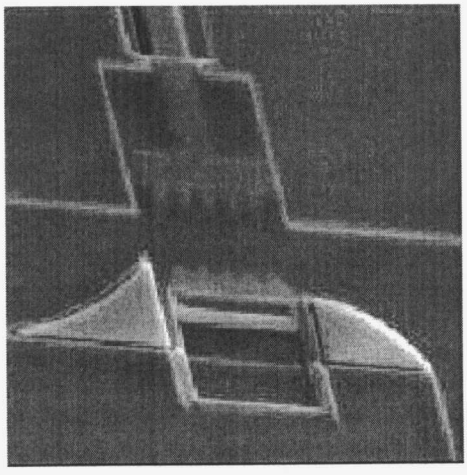

Figure 5: Cellular manipulation device which shows the integration of microfluidic channels and mechanical structures. The width of the channel is 12.5 um at the narrowest point for this design variation.

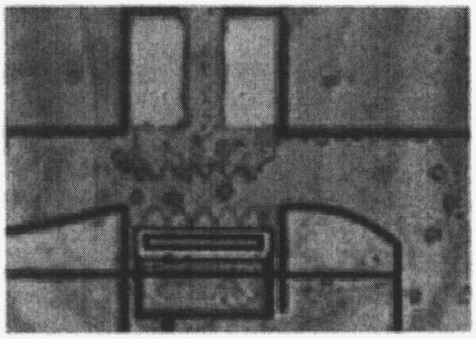

Figure 6: Red blood cells flowing through the cellular manipulation device.

The manipulator is designed to disrupt the cell membrane to allow delivery of large molecules into the cell. Other devices include flow channels with electrodes arranged around the channel to create and sense electric and magnetic fields (Fig.7).

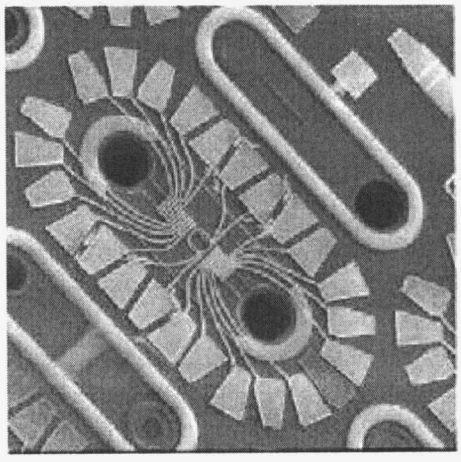

Figure 7: A flow channel with electrodes for creating/sensing electric and magnetic fields. Electrodes with varying shapes and spacing allow creation of almost any arbitrary field inside the channel.

In a system view, integration of MEMS components similar to the ones shown here will allow multiple complex functions to be performed on a chip. This capability will push the level of system integration to a smaller scale and enhance the manufacturability and applicability of microfluidic and BioMEMS microsystems. The hybrid integration of these components with plastic and/or glass based components is also a key enabler for bridging the meso-micro-nano domains in order to create the truly integrated systems.

REFERENCES

[1] see http://www.mdl.sandia.gov/micromachine for bibliography.

[2] P Galambos, K Zavadil, R Givler, F Peter, A Gooray, G Roller, and J Crowley, "A Surface Micromachined Electrostatic Drop Ejector", Transducers '01, June 2001 (submitted).

[3] M Stay, "Simulation, Design and Performance of Surface Micromachined Peristaltic Pumps", Masters Thesis, University of Colorado, Dept. of Chemical Engineering, December 2000.

A MEMS Device for Measurement of Skin Friction with Capacitive Sensing

Jiang Zhe, K. R. Farmer* and Vijay Modi

Dept. of Mechanical Engineering, Columbia University, New York, NY 10027

* Microelectronics Research Center, New Jersey Institute of Technology, Newark, NJ 07102

Abstract-**A microfabricated floating-element sensor for the measurement of wall shear stress is developed. The design objective is to measure shear stress in the range of 0.1 to 2 Pa, with a spatial resolution of O(100 μm). The sensor is micromachined in an ultra-thin silicon wafer using wafer bonding and DRIE techniques. Preliminary test results have been obtained by applying an electrostatic force to the sensor instead of a fluid force. The floating element deflection is then measured using direct and differential capacitance techniques as well as an optical method for additional confirmation of the results. These test results have been compared to theoretical simulations using MEMCAD software. The results show that with this sensor design it is possible to measure a shear force as small as 5 nN ± 0.5 nN, corresponding to a shear stress level of 0.05 Pa ± 0.005 Pa.**

I. Introduction

The measurement of shear is of great interest since shear is the primary means of interaction between a flow and the solid surface. The initial motivation for this particular study arose from the need to measure the shear stress footprint of turbulent impinging jets [1] in a fountain plater (used for electrochemical deposition of copper) with a high spatial resolution. However, direct measurement of shear stress with a high spatial resolution (of say 100 μm) is difficult because of the low level of forces involved. An impinging jet system with a jet width of O(1 cm), would require an ability to measure a force of several nano-Newtons on a 100 μm by 100 μm plate for a jet Reynolds numbers of $O(10^4)$.

The first floating-element MEMS shear sensors were reported by the MIT group [2, 3, 4] using piezoresistive, capacitive and optical techniques. They report the highest detection sensitivity with an optical measurement technique. A MEMS sensor was developed by the group at Case-Western [5, 6] using a folded-beam spring structure to obtain higher deflection sensitivity. They employ monolithic integration of an on-chip circuit (based on the ADXL design), with the mechanical sensor adding considerably to the complexity of fabrication.

The goal of the present work was to develop a sensor that does not require optical access and can be used for research purposes with existing off-sensor circuitry and electronics. The present MEMS based sensor was developed to work with direct (using an LCR meter) or differential (using a MS3110 chip) capacitance measurement techniques. Using a single cantilever beam a deflection sensitivity of approximate 1 μm/Pa is achieved. The output sensitivities are 20 fF/Pa and 0.5 V/Pa for direct and differential capacitance measurements, respectively.

II. Sensor Design

The floating-element sensors developed in this study are based on a cantilever-beam-like structure as shown in Fig. 1 (top view). The device is designed to be laterally (in-plane) soft and vertically (out-of-plane) stiff, with beam width b of 10 μm, much smaller than the vertical dimension of about 50 μm, the thickness of the ultra-thin wafer. Two sense electrodes shown as S and S' in Fig. 1 are located at the two sides of the floating element F, separated by a 5 micron trench. Two actuation electrodes shown as E and E' in Fig. 1 are positioned on both sides of the upper portion of the beam with a separation of 25 μm from the beam. The purpose of the actuation electrodes is to provide the ability to apply a low level electrostatic force on the beam for testing the device in the absense of a fluid flow. With a cantilever beam length L of 3 mm, a spring constant of 80 nN/μm is achieved. Fig. 2 shows the floating element portion of a fabricated sensor with width, n_1, of 200 μm and length, n_2, of 500 μm (n_1 and n_2 are shown in Fig. 1). A floating element of this size would experience shear forces of 10 to 50 nN in the 0.1 to 0.5 Pa shear stress range.

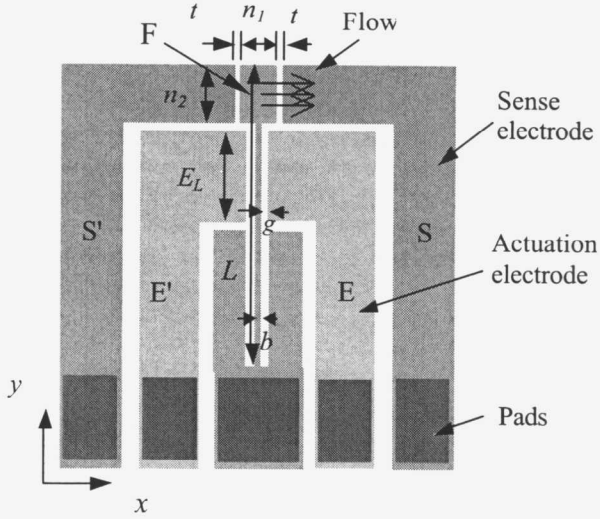

Fig. 1 Schematic top view sketch of the entire sensor.

0-7803-7224-7/02/$17.00 © 2002

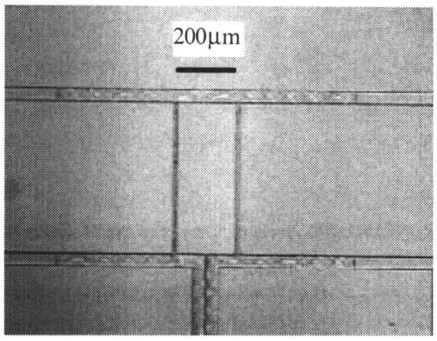

Fig. 2 Top view of the fabricated device showing the floating element and a portion of the cantilever beam.

III. Microfabrication

Microfabrication of the shear sensor was carried out in the Microelectronics Research Center at New Jersey Institute of Technology. The fabrication begins with a 4 μm deep KOH etch to provide release windows in a 4" diameter, 500 μm thick substrate wafer. Next both the thin (50 μm) and the substrate wafers are oxidized and then bonded together using fusion bonding. After bonding, we wet etch the top layer of silicon dioxide and deep reactive ion etch through the thin wafer to define the desired floating parts. However, at this stage the floating element is still not released because of the presence of SiO_2 at the bond interface. In the next step, a gold evaporation and liftoff are used to define contact pads. Finally the free structures are released, and wire bonding is used to create the test device. The detailed step by step process is sketched in Fig. 3.

IV. Testing And Results

A. Direct Capacitance Measurement

The wire bonded sensor is mounted on a small PC board and placed within a shielding box to minimize the noise. The sensor was first tested by applying a DC voltage ranging from 1 V to 5 V between the floating element F and the left sense electrode S' to generate an electrostatic force on F. The relationship between this applied voltage and the generated force was obtained using a MEMCAD simulation and is shown in Fig. 4. The change in the capacitance (between S' and F) due to this force is then measured using an HP 4284A precision LCR meter. The relationship between capacitance change and the applied voltage is also shown in Fig. 4. With an observed resolution of 1 fF at a 10 pF level with the LCR meter, it is possible to measure forces as small as 100 nN ± 10 nN using this technique.

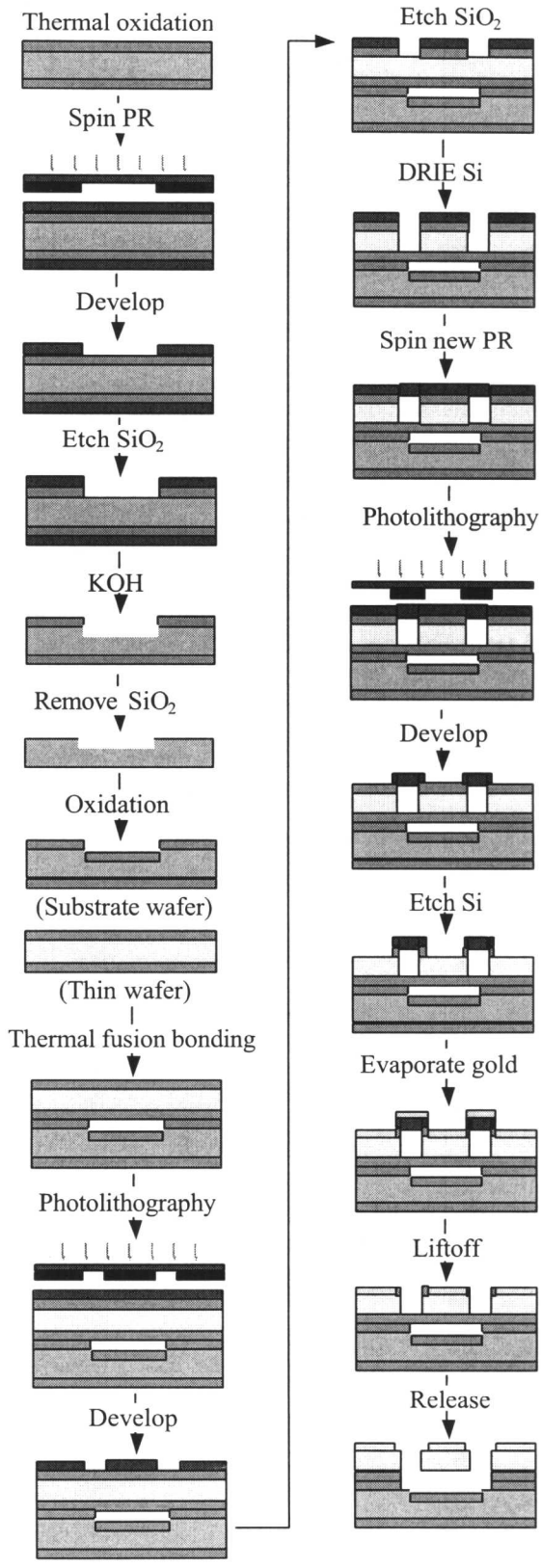

Fig. 3 Sensor microfabrication process.

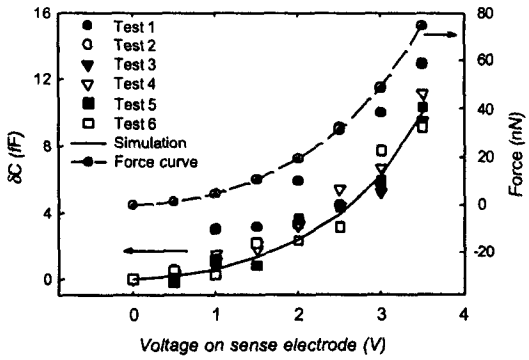

Fig. 4 The relationships between applied voltage and force (right axis) and the relationship between applied voltage and capacitance change (left axis).

B. Deflection Measurement

In order to independently ascertain whether the applied voltage is indeed a reasonable way to apply a force, the deflection of the floating element is also measured with a WYKO optical profilometer with a lateral resolution of ±0.1μm. Tests are carried out with applied voltages between F and S' and between E' and F. The measured as well predicted deflection-voltage relationship for S' and F is shown in Fig. 5(a). The agreement between the optically measured deflection and the prediction is very good to within the uncertainty of the opical measurment. A similar test for E'-F electrodes is shown in Fig. 5(b), allowing better exploration of the low deflection region. The agreement in the low deflection is also very good.

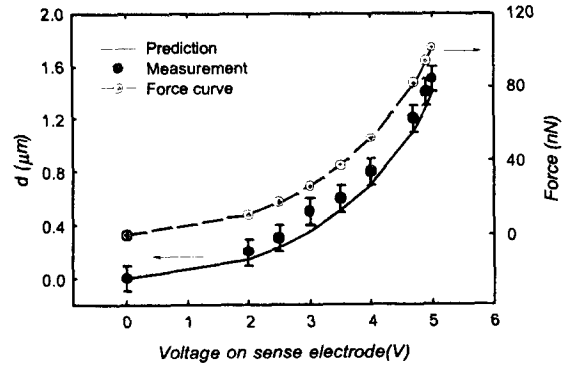

Fig. 5 (a) Profilometer measurements of deflection with applied voltages between S' and F.

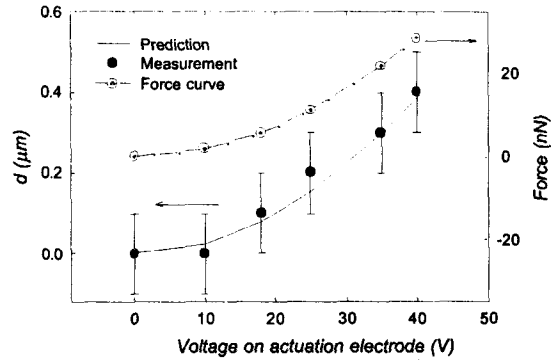

Fig. 5 (b) Profilometer measurements of deflection with a voltage applied between E' and F.

C. Differential Capacitance Measurement

The sensor was then tested using a differential-capacitance measurement technique using an off-the-shelf MS3110 Universal Capacitive Readout™ IC. The MS3110 chip senses the change in the differential capacitance between two capacitors and provides an output voltage propotional to that change [9], eliminating the problem of a large parasitic capacitance associated with the direct measurement of capacitiance. For these tests a voltage was applied between E' and F. The differential capacitiance measured is the difference of *CS1* (between S and floating element) and *CS2* (between S' and floating element). The change in *CS1-CS2* before and after the voltage is applied is given by $\delta C=\delta$ *(CS1-CS2)*. The change in output voltage δV_{out} is linearly proportional to the change δ(CS1-CS2):

$$\delta V_{out} = G * \delta(CS2 - CS1) / CF \qquad (1)$$

where G is 10.26 volts and CF is selected to optimize the input sense capacitance range, and is set to 266 fF for the present measurement [9].

The results of measured change δC due to an applied voltage converted to an equivalent force are shown in Fig 7. The results show a linear behavior as expected when the deflection is small compared to the initial gap between the capacitors. These results translate into an output voltage sensitivity of approximately 20 mV/fF for an initial separation of 7 μm. The gap was measured independently using a profilometer. With an uncertainty of 0.5 fF in δC (due to a 10 mV observed uncertainty in δV_{out}) the uncertainties in the force and shear measurements are 0.5 nN and 0.005 Pa, respectively. Hence for a 10% uncertainty we can anticipate making measurements of shear forces as small as 5nN corresponding to a shear stress level of 0.05 Pa. The maximum force that can conceivably be measured with the present sensor is limited by the maximum deflection and is expected to be 160 nN for a 2 μm deflection.

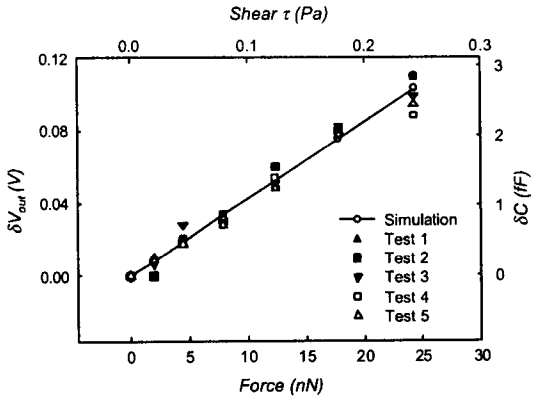

Fig. 7 Variation in experimental and simulated output voltage changes with electrostatic force by differential capacitance measurement.

V. Conclusions

A sensitive MEMS based shear stress sensor has been developed to measure forces as small as 5 nN in the plane of the sensor without using optical means. The sensing mechanism is capacitive, and the technique utilizes off-the-shelf electronic components external to the mechanical sensor. The preliminary tests of the sensor have been carried out using an electrostatic force applied to the sensor. Future work will address tests using a wall shear stress due to a fluid flow.

Acknowledgment

This work was partially supported by NSF under grant CTS-9706824, and by the NJ Commission on Science and Technology through the NJ MEMS Initiative. We gratefully acknowledge the assistance provided by Dr. Suresh Sampath and Dr. Zhixiong Xiao of Microelectronics Research Center at New Jersey Institute of Technology and discussions with Prof. Luc Frechette of Columbia University.

References

[1] J. Zhe, and V. Modi, "Near-wall measurements for a turbulent impinging slot jet system," ASME *Journal of Fluids Engineering*, Vol. 123, No.1, pp 112-120.

[2] J. Shajii, K. Y. Ng and M. A. Schmidt, A microfabricated floating-element shear stress sensor using wafer-bonding technology, *J. MEMS*, pp.89-94, 1992.

[3] A. Padmanabhan, H. D. Goldberg, K. S. Breuer, M. A., Schmidt, A Silicon Micromachined floating-element shear-stress sensor with optical position sensing by photodiodes, *8th International Conference On Solid State Sensors and Actuators,* Stockholm, Sweden, Jun 25-29, pp. 436-439, 1995.

[4] M. A. Schmidt, R. T. Howe, S. D. Senturia, and Haritonidis, J.H., Design and calibration of a microfabricated floating-element shear-stress sensor, *IEEE Transactions on Electron Devices*, vol. 35, No.6, 750-757, June 1988.

[5] T. Pan, D. Hyman, M. Mehregany, E. Reshotko, and S. Garverick, Microfabricated shear stress sensors, Part 1: design and fabrication, *AIAA Journal*, vol. 37, No. 1, pp. 68-72 January 1999.

[6] D. Hyman, T. Pan, E. Reshotko, M. Mehregany and S. Garverick, Microfabricated Shear Stress Sensors, Part 2: Testing and Calibration, *AIAA Journal*, vol. 37, No. 1, pp. 73-78, January 1999.

[7] G. T. A. Kovacs,, Micromachined Transducers Source Book, WCB/McGraw-Hill, 1998.

[8] D. O. Brush, and B. O. Almroth, Buckling of Bars, Plates and Shells, McGraw-Hill, 1975.

[9] Micro Sensors Inc., MS3110 Universal Capacitive Readout™ IC and Evaluation/Programming Manual, 2001.

[10] S. Timoshenko, Strength of Materials-Part2: Advanced Theory and Problems, 3rd ed. New York: Van Nostrand, 1956.

Microfluidic electrowetting-based droplet mixing

Vamsee K. Pamula[Ψ], *Member*, Philip Y. Paik, Jai Venkatraman, Michael G. Pollack, *Member*, and Richard B. Fair, *Fellow, IEEE*,

Department of Electrical Engineering, Duke University, Durham, NC 27708

Abstract- **We present a liquid droplet mixer to enable mixing of the samples and reagents for chemical and biological analysis in micro total analysis systems (μTAS). The droplets in the mixer are actuated based on electrowetting phenomenon. The actuator comprises of two parallel glass plates between which the droplet is actuated on a planar array of electrodes. Mixing of liquid channels in microfluidic systems has been demonstrated for continuous flow systems where the mixing is diffusion-limited due to the laminar flow of liquids, requiring very long, thin channels.**

In the present paper, mixing is performed on discrete droplets of liquid. When two droplets are brought together, depending on the velocity of the moving droplets, surface tension, viscosity, electrode activation, and volume among other factors, turbulence is created which aids in mixing. The mixing is not limited by diffusion and enhanced by transport. The mixing experiments are performed between fluorescein and plain water droplets whose individual volume is 1.75μl. Mixing is visualized with a 2-CCD camera setup to observe both the top and side views, with appropriate filters to capture fluorescence. We observed that it takes about 60 seconds for two droplets of 1.75μl each to mix when their surface tensions are different and it takes about 90 seconds when the two droplets have similar surface tensions. The present mixer stands apart from any current conventional micromixers in that the mixing times occupies much lesser area, mixing does not need any specific architecture on the chip and can be performed on any transport electrodes dynamically assigned to mixing.

Index Terms— **Droplet, electrowetting, fluorescence, microfluidics. mixing**

I. Introduction

MIXING .in microfluidic devices is one of the critical steps in realizing a μTAS (micro total analysis system) or for "lab on a chip" systems. Mixing requirements can be either in dilution of the samples before analysis or in mixing the samples with reagents in a particular ratio. The ability to mix liquids rapidly and utilizing minimum area, greatly improves the throughput of such systems.

We present a microfabricated electrowetting actuator that can be used to perform mixing, transport, and dispensing. Electrowetting is the process by which the interfacial tension between a liquid and solid phase is modulated electrically [1]. This device has all the advantages of a microfluidic system such as the ability to handle small volumes, high throughput, rapid transport, and batch fabrication. However, liquid is handled as droplets enabling discrete manipulation unlike conventional continuous flow microfluidic devices. Since the liquid is handled as droplets, just the right volume required for a reaction can be utilized thereby reducing the dead volume. In this paper, we present some preliminary results obtained on mixing in this device.

Mixing in microfluidics is performed either by turbulence or through interdiffusion. Since the Reynolds numbers are very low for continuous flow systems, mixing relies mainly on the interdiffusion in the channels. Several researchers have tried various approaches to create turbulence in the flow streams to promote mixing. Hosokawa et al. have demonstrated mixing of droplets in a hydrophobic microcapillary valve device where the droplets are formed, actuated, and mixed with the help of air pressure [2]. They mixed two droplets of fluorescein and deduced mixing from the fluorescence intensity measurements obtained from the top view. In this paper, we show the profiles both from top and side view to get a more complete picture of the mixing process as it occurs. In our device, due to the nature of the motion of the droplet, which is not clearly understood yet, mixing is enhanced.

II. Experimental

The droplets are actuated by electrowetting phenomenon in which their surface tension is controlled electrically as demonstrated by Pollack et al [3]. A droplet of polarizable and conductive liquid is sandwiched between two planar electrodes. The bottom plate consists of an array of independently addressable chrome control electrodes coated with Parylene C (800 nm) for insulation while the top plate coated with Indium Tin Oxide (ITO) acts as a ground electrode. Both the electrode surfaces are coated with a thin hydrophobic layer of Teflon AF 1600 (50 nm). The top and bottom plates were separated by a glass spacer yielding a fixed gap.

Each droplet is made to contact both the top and bottom

[Ψ] vkp@ee.duke.edu

0-7803-7224-7/02/$17.00 © 2002

electrodes. The volume of the droplet is chosen to overlap the two adjacent bottom electrodes slightly. The sides of the bottom electrodes are interdigitated to increase the overlap of the droplet. The droplet is surrounded by either just ambient air or silicone oil, which is immiscible with the droplet. A custom control system was made to address and switch each electrode. Since this actuation does not need any fixed channels or moving parts, any electrodes on the chip can be designated for mixing.

The schematic of the droplet actuation for mixing is shown in top and side view in Fig.1. A droplet containing fluorescein is actuated towards a non-fluorescein droplet. The fluorescein droplet contains 1mM fluorescein (obtained from JT Baker) for fluorescence, 0.125M KCl for making the droplet conductive, and 0.125M NaOH since the fluorescence of fluorescein is pH – dependent. The non-fluorescein droplets contain 0.125M KCl and 0.125M NaOH or just 0.125 M KCl. All the droplets were made in deionized water.

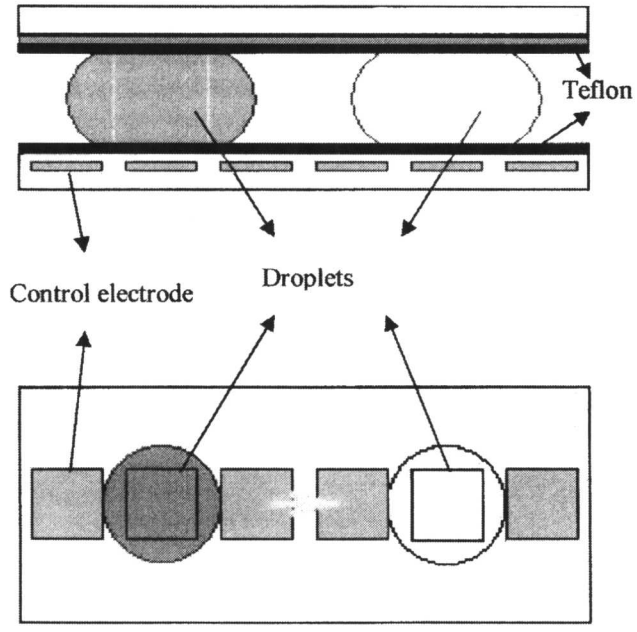

Figure 1 Schematic side and top view of the electrowetting-based mixing actuator

Either the fluorescein droplet is moved towards the non-fluorescein droplet or vice versa. The resulting motion is captured on a video through a CCD camera. A two-camera setup was used to get both the top and side view of the mixing process simultaneously as shown in Fig. 2. The fluorescein droplet was excited with a tungsten lamp with a blue filter (490 nm). Both the cameras were mounted with long pass filters (>510 nm) to collect the fluorescence. The videos were then digitized for further analysis.

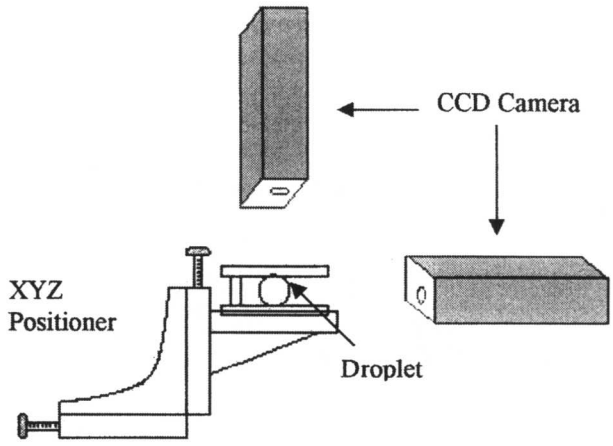

Figure 2 Two CCD camera setup to view top and side view of droplet mixing

The interfacial tension of a fluorescein droplet, containing 0.1mM fluorescein and 0.125M NaOH and KCl, with 1cSt silicone oil is measured to be 37 dynes/cm whereas a non-fluorescein droplet, containing only NaOH and KCl both at 0.125M, has 36 dynes/cm with the same oil. The viscosity for fluorescein and non-fluorescein droplets is 1.396 and 1.373 cP and the conductivity is 29.7 mMho & 25.9 mMho, respectively. The interfacial tension of a 0.125M KCl droplet is 31.4 dynes/cm with 1 cSt silicone oil.

III. Results and Discussion

A number of parameters can be varied to study their effect on mixing in our current setup. For the initial experiments, we have chosen to fix the gap between the top and the bottom electrodes (i.e., the droplet height) at 800 μm and the pitch of the bottom electrodes as 1.5 mm, which fixes the volume of the droplet. The volume of each droplet was fixed at 1.75 μl in all the experiments. The voltage of actuation for the moving droplet also is fixed at 30V since the voltage affects the speed of the impinging droplet and thereby the mixing. All the experiments were performed with the surrounding medium of 1 cSt silicone oil.

Initially a fluorescein droplet containing fluorescein, NaOH and KCl (designated as F) was moved onto a non-fluorescein droplet containing NaOH and KCl (NF) with the appropriate activation of the sequence of electrodes as shown in Fig.1. The electrode adjacent to NF droplet is switched on and off for a very small amount of time for the F droplet to move onto the NF droplet so that both the F and NF droplet finally occupy the same electrode which NF was initially occupying. In this case, there is a very small difference in the interfacial tension of the droplets with oil. Even though the droplets look

mixed from the top view in about 15 seconds, the view from the side reveals that F droplet has just gone underneath the NF droplet as shown in Fig. 3. Mixing proceeds through diffusion from this point and it takes about 90 seconds to completely mix.

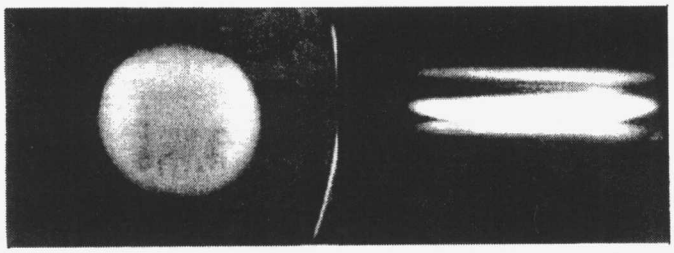

Figure 3 Top and Side views of a fluorescein droplet mixing with a non-fluorescein droplet at 15 seconds after coalescence.

If the initial coalescence does not create enough turbulence for mixing then we observe that the F droplet and NF droplet are vertically separated. At this point, the mixing is just diffusion limited. To enhance the mixing rate, the area of contact was increased. Experiments were performed similar to the previous one but the difference being the coalescence occurs on two electrodes instead of one electrode. The F and NF droplet come together on two electrodes which doubles the area of contact compared to the previous case. We do not observe a significant change in the mixing times in this case.

In the next set of experiments, we moved an F droplet towards a KCl droplet (which has just 0.125M KCl). It was repeatedly observed that the F droplet would just engulf the KCl droplet while the droplets are coalescing. From the side view, it would appear as if mixing is complete since the KCl droplet is completely engulfed by the F droplet. However, from the top view we observed that the F droplet forms a ring around the KCl droplet yielding a donut shape as shown in Fig 4. Within 10 seconds, uniform fluorescence can be observed from the top but from the side view it appears that fluorescein goes underneath the KCl droplet as shown in Fig. 5. From now on, mixing seems to occur by diffusion. Uniform fluorescence appears from the side in 1 second, from the top in 10 seconds, and again from the side in 60 seconds from the start of coalescence.

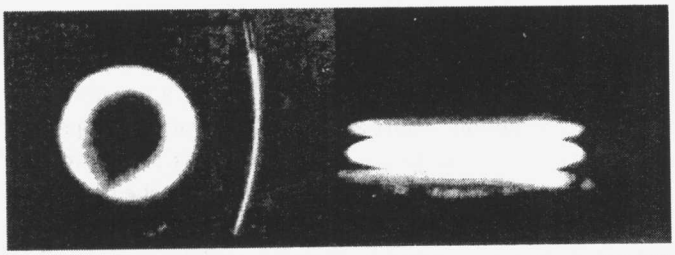

Figure 4 Top and side views of a fluorescein and KCl droplet immediately after coalescence.

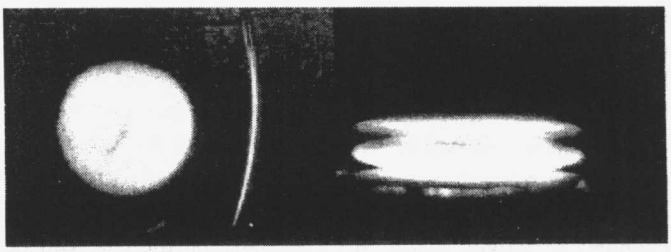

Figure 5 Top and side views of a fluorescein and KCl droplet 10 seconds after coalescence

A similar experiment was performed with the KCl droplet moving into the Fluorescein droplet. In this case, the droplets just come together and there is no engulfment as in Fig. 4. Nevertheless, it takes just about the same time for mixing to finish. It appears that mixing is faster in droplets, whose surface tensions are very different. When the surface tensions are similar then it takes about 90 seconds (1.5 times more than surface tension mismatched case) for mixing to finish and when the surface tensions are similar and the coalesced droplet is spread on two electrodes then it takes 180 seconds (3 times more than surface tension mismatched case) for mixing to finish.

It should be noted that we are observing only from two angles, which may not yield sufficient information. Ideally, we would like to get a 3D view of the droplet while it is mixing to see if there are any unmixed volumes in the coalesced droplet, which cannot be made out by just looking at the surface of the droplets from all angles.

REFERENCES

[1] G. Beni and S. Hackwood, "Electro-wetting displays," Applied Physics Letters, Vol 38, pp. 207-209, (1981)

[2] K. Hosokawa, T. Fujii, and I. Endo, *"Formation and active mixing of metered nano/picoliter liquid droplets in a microfluidic device,"* 4th International Symposium on Micro Total Analysis Systems 2000.

[3] M.G. Pollack, R.B. Fair, A.D. Shenderov, *"Electrowetting-based actuation of liquid droplets for microfluidic applications,"* Applied Physics Letters, Vol. 77, no. 11, pp. 1725-1726, (2000).